Ab initio investigation of BCS-type superconductivity in $LuNi_2B_2C$-type superconductors

H. M. Tütüncü,[1,2] H. Y. Uzunok,[1,2] Ertuğrul Karaca,[1] G. P. Srivastava,[3] S. Özer,[1] and Ş. Uğur[4]

[1]*Sakarya Üniversitesi, Fen-Edebiyat Fakültesi, Fizik Bölümü, 54187 Sakarya, Turkey*

[2]*Sakarya Üniversitesi, Biyomedikal, Manyetik ve Yarıiletken Malzemeler Araştırma Merkezi (BIMAYAM), 54187 Sakarya, Turkey*

[3]*School of Physics, University of Exeter, Stocker Road, Exeter EX4 4QL, United Kingdom*

[4]*Gazi Üniversitesi, Fen Fakültesi, Fizik Bölümü, Teknikokullar, Ankara, Turkey*

(Received 9 June 2015; published 20 August 2015)

Ab initio pseudopotential calculations have been made to calculate the structural, electronic, vibrational, and superconducting properties of the borocarbide superconductors RM_2B_2C (R = Lu,La,Y; M = Ni,Pd,Pt). Using the electronic and vibrational spectra, the average electron-phonon coupling parameter is calculated to be 0.78, 0.83, 0.96, and 1.48 for $LaPt_2B_2C$, $LuNi_2B_2C$, YPt_2B_2C, and YPd_2B_2C, respectively. From a detailed spectral analysis throughout the irreducible Brillouin zone (IBZ), we found that the highest contribution to the electron-phonon coupling parameter for these materials comes from the acoustic and low-frequency optical modes characterized with anomalous dispersion, instead of the A_{1g} optical-phonon mode claimed in previous studies. Using the calculated electron-phonon coupling parameter values, the superconducting critical temperatures for $LaPt_2B_2C$, $LuNi_2B_2C$, YPt_2B_2C, and YPd_2B_2C are found to be 10.40, 15.94, 11.30, and 20.60 K, respectively, which are in good accordance with their experimental values of 10.50, 16.10, 10.00, and 21.00 K.

DOI: 10.1103/PhysRevB.92.054510 PACS number(s): 63.20.kd, 71.15.Mb, 74.25.Kc

I. INTRODUCTION

The discovery of superconductivity in the borocarbide systems RM_2B_2C (R = Y,Sc,rare earth; M = Ni,Pd,Pt) with critical temperature up to 23 K has refreshed interest in intermetallic superconductivity [1–20]. The development of superconductivity in these compounds with the existence of the transition metals Ni and Pd, which are generally magnetic in intermetallic compounds, is especially interesting. The structural, electronic, and superconducting properties of these compounds have been studied experimentally over the past several years, in part due to their high superconducting temperatures [21–45]. In particular, heat capacity measurements [7–9,15] show that a BCS-type scenario, with a strong electron-phonon coupling strength, is the most appropriate theoretical description for these superconductors. Moreover, a significant boron isotope effect has been observed for YNi_2B_2C and $LuNi_2B_2C$, corroborating the classification of these compounds as phonon-mediated superconductors [46,47].

A detailed study of the vibrational properties of superconductors is as important as their electronic properties, since phonons essentially are responsible for the coupling between electrons to form Cooper pairs required in the BCS theory. Hadjiev and co-workers [48] reported micro-Raman spectra of YNi_2B_2C at room temperature. Inelastic-neutron-scattering curve techniques [49] were used to measure the low-lying phonon dispersion $LuNi_2B_2C$ along the [100] and [001] symmetry directions, while Raman measurements on RNi_2B_2C (R = Lu, Ho, and Y) single crystals were reported in the experimental work of Park *et al.* [50]. Recently, Weber and co-workers [51] presented an inelastic neutron-scattering investigation of phonons with energies up to 159 meV (38 THz) in the conventional superconductor YNi_2B_2C.

Considerable progress has been made toward the theoretical description of the electronic properties of $LuNi_2B_2C$. The linear augmented-plane-wave (LAPW) method [52–54] and the augment-spherical-wave (ASW) method [55] have been used to calculate the electronic structure of $LuNi_2B_2C$. These calculations [52–55], based on the local-density approximation (LDA), show that, unlike the cuprate high-temperature superconductors, $LuNi_2B_2C$ is a three-dimensional metal with all atoms contributing to the metallic character. The electronic properties of $LaPt_2B_2C$ have been investigated using a local orbital extension of the general potential LAPW method [56]. This work indicates that the crystal structures, physical properties, and ion valences of $LaPt_2B_2C$ and $LuNi_2B_2C$ are similar, remarking that the superconductivity of these materials has a similar origin as well. Following these theoretical works [52–56], the electronic properties of $LuNi_2B_2C$ have been investigated by means of the *ab initio* plane-wave pseudopotential method within local-density-functional theory [57]. This work claims that the superconductivity found in $LuNi_2B_2C$ may be based on the conventional mechanism rather than an exotic one. The effect of pressure on the compressibilities of $LuNi_2B_2C$ and YPd_2B_2C has been studied within the local-density approximation to density-functional theory [58,59]. These LDA calculations [58,59] confirm the three-dimensional metallic character of these superconductors. *Ab initio* frozen-phonon calculations are used to calculate zone-center phonons in $LuNi_2B_2C$ using the generalized-gradient-corrected full-potential LAPW method [60]. Reichardt *et al.* [61] presented first-principles calculations of the electronic band structure, the phonon-dispersion relations, and the electron-phonon interaction in YNi_2B_2C within the LDA. The prediction of Mattheis and co-workers [53] of a considerable electron-phonon coupling of the zone-center A_{1g} mode is affirmed by the work of Reichardt *et al.* [61]. However, they show that the electron-phonon coupling of this phonon mode decreases rapidly with increasing wave vector [61]. They clearly point out that the contribution of this phonon mode to the average electron-phonon coupling parameter (λ) is only 4%, while about 70% of λ comes from low-frequency optical-phonon modes and acoustic-phonon modes. In our

recent *ab initio* work [62], we have made a similar observation for the electron-phonon interaction in YPd_2B_2C.

Although the structural and electronic properties of $LuNi_2B_2C$, YPd_2B_2C, $LaPt_2B_2C$, and YPt_2B_2C have been studied theoretically, no systematic attention has been paid toward the vibrational properties of these superconductor materials. Lack of information regarding phonon-dispersion relations precludes direct calculation of the electron-phonon coupling parameter and the superconducting transition temperature (T_c). Thus, in order to understand the origin of superconductivity in these compounds, their structural, electronic, phonon, and electron-phonon interaction properties must be studied in detail. For this reason, this work is aimed at making *ab initio* calculations of the structural, electronic, and phonon properties of these superconductors by using a generalized gradient approximation (GGA) of the density-functional theory. The calculated lattice parameters (a and c), electronic properties, phonon-dispersion curves, and density of states for these materials have been presented and discussed. With these results, the Eliashberg spectral function, the average electron-phonon coupling constant λ, the logarithmic average frequency $\omega_{\ln}$, and the superconducting critical temperature T_c for these compounds are computed and compared with available experimental reports.

II. THEORY

Our calculations are performed using the QUANTUM ESPRESSO code [63], which is based on a plane-wave expansion of the electronic wave functions for a crystal structure with periodic boundary conditions. We describe the electronic exchange-correlation terms using the generalized gradient approximation (GGA) and the Perdew-Burke-Ernzerhof functional [64]. Electron-ion interactions are taken into account using the pseudopotential method. We note that on the QUANTUM ESPRESSO home page, both norm-conserving pseudopotentials [65] as well ultrasoft pseudopotentials [66,67] are available for all the elements required for the present study, but only norm-conserving pseudopotentials are available for Lu. Thus, we chose to use ultrasoft potential for all the elements in YPd_2B_2C, $LaPt_2B_2C$, and YPt_2B_2C. However, for the sake of not mixing norm-conserving and ultrasoft potentials for the elements in $LuNi_2B_2C$, we employed the norm-conserving pseudopotentials. Single-particle wave functions are expanded in a plane-wave basis, with a kinetic-energy cutoff of 60 Ry. Self-consistency in solutions to the Kohn-Sham equations [68] is acquired by considering four $\boldsymbol{k}$ points within the irreducible Brillouin zone (IBZ). The energy calculations in the IBZ are performed with an $(8 \times 8 \times 8)$ $\boldsymbol{k}$-point mesh using the Monkhorst-Pack scheme [69]. On the other hand, the $\boldsymbol{k}$-point mesh that is used for the electronic calculations in the IBZ is taken as $24 \times 24 \times 24$.

The first-principles investigations of the phonon frequencies and atomic displacements are made using a linear-response method [63]. The screening of the electronic system in response to the displacement of the atoms is taken into consideration in a self-consistent manner. Thirteen dynamical matrices are calculated using a mesh of (4, 4, 4) reciprocal lattice divisions. These dynamical matrices are Fourier-transformed to calculate the full phonon spectrum and density of states using the Monkhorst-Pack $8 \times 8 \times 8$ $\boldsymbol{k}$-points grid within the IBZ.

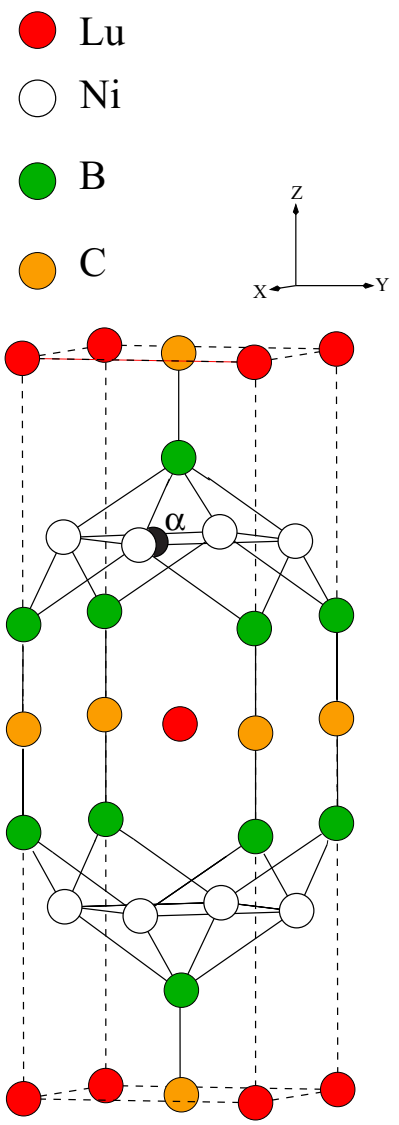

FIG. 1. (Color online) The body-centered-tetragonal structure of $LuNi_2B_2C$.

Our electronic and phonon results, together with the linear-response method for the determination of the electron-phonon coupling and the Eliashberg function, have made it possible to calculate the superconducting transition temperature T_c and study electron-phonon interaction in detail. The Eliashberg electron-phonon spectral function $\alpha^2F(\omega)$ can be expressed as [70–79]

$$\alpha^2 F(\omega) = \frac{1}{2\pi N(E_F)} \sum_{\boldsymbol{q}j} \frac{\gamma_{\boldsymbol{q}j}}{\hbar\omega_{\boldsymbol{q}j}} \delta(\omega - \omega_{\boldsymbol{q}j}), \qquad (1)$$

where $N(E_F)$ is the electronic density of states at the Fermi level, and $\gamma_{\boldsymbol{q}j}$ is the phonon linewidth for mode $\boldsymbol{q}$. When the electron energies around the Fermi level are linear in the range of phonon energies, the phonon linewidth is given by Fermi's

TABLE I. Structural parameters for $LaPt_2B_2C$, YPd_2B_2C, YPt_2B_2C, and $LuNi_2B_2C$ and their comparison with previous experimental and theoretical results.

Material	a (Å)	c (Å)	V (Å^3)	z	$d_{M\text{-}M}$	$d_{\text{B-C}}$ (Å)	$d_{M\text{-B}}$ (Å)	$\alpha_{\text{B-}TM\text{-B}}$	B (GPa)	B′
$LaPt_2B_2C$										
Present GGA work	3.904	10.773	82.09	0.362	2.761	1.485	2.296	106.09°	188.6	4.65
Experimental [12]	3.868	10.705	80.08	0.362	2.735	1.480	2.274	106.06°		
YPd_2B_2C										
Present GGA work	3.807	10.745	77.86	0.363	2.692	1.471	2.258	106.84°	203.5	4.01
LDA [59]	3.760	10.719	75.77						228.0	
Experimental [13]	3.710	10.810	74.39							
Experimental [25]	3.760	10.740	75.91							
YPt_2B_2C										
Present GGA work	3.809	10.818	78.47	0.364	2.694	1.475	2.267	107.10°	170.0	4.62
Experimental [16]	3.79	10.710	76.92							
$LuNi_2B_2C$										
Present GGA work	3.508	10.597	65.20	0.360	2.481	1.485	2.105	107.80°	185.1	4.08
LDA [58]	3.457	9.989	59.69						210.0	
Experimental [12]	3.464	10.631	63.78	0.362	2.449	1.468	2.101	108.69°		
Experimental [14]	3.467	10.633	63.90							
Experimental [21]	3.464	10.623	63.73							
Experimental [22]	3.464	10.635	63.81							
Experimental [23]	3.464	10.623	63.73							
Experimental [31]	3.464	10.631	63.78							

"golden rule" formula [72,73,75–79]

$$\gamma_{\mathbf{q}j} = 2\pi\omega_{\mathbf{q}j}\sum_{\boldsymbol{knm}}\left|g^{\boldsymbol{q}j}_{(\boldsymbol{k}+\mathbf{q})m;\boldsymbol{kn}}\right|^2\delta(\varepsilon_{\boldsymbol{kn}}-\varepsilon_F)\delta(\varepsilon_{(\boldsymbol{k}+\boldsymbol{q})m}-\varepsilon_F), \tag{2}$$

where the Dirac δ functions express energy conservation conditions. The electron-phonon matrix element g is given as [75–79]

$$g^{\boldsymbol{q}j}_{(\boldsymbol{k}+q)m;\boldsymbol{kn}} = \sqrt{\frac{\hbar}{2M\omega_{\boldsymbol{q}j}}}\langle j,\boldsymbol{k}+qm|\Delta V^{\text{SCF}}_{\boldsymbol{q}}|i,\boldsymbol{kn}\rangle, \tag{3}$$

where $|i,\boldsymbol{k}\rangle$ is the Bloch electron eigenstate with the wave vector $\boldsymbol{k}$, band index i, and energy $E_{i,\boldsymbol{k}}$; $\Delta V^{\text{SCF}}_{\boldsymbol{q}}$ [79] is the derivative of the self-consistent effective potential with respect to the atomic displacements caused by a phonon of frequency ω with wave vector $\boldsymbol{q}$; and M is the atomic mass. The electron-phonon coupling parameter (λ) is calculated from [75–78]

$$\lambda = 2\int\frac{\alpha^2F(\omega)}{\omega}d\omega. \tag{4}$$

The summations in Eqs. (1) and (2) are performed using a dense mesh [$(24\times24\times24)$ Monkhorst-Pack mesh] of $\boldsymbol{k}$ points in the IBZ.

III. RESULTS

A. Structural and electronic properties

The RM_2B_2C compounds assume the $LuNi_2B_2C$-type body-centered-tetragonal crystal structure belonging to the space group $I4/mmm$. This structure, illustrated in Fig. 1, includes one molecule with six atoms per unit cell, with Lu (Y,La) located at $2a(0,0,0)$, Ni (Pt,Pd) at $4d(0,1/2,1/4)$, B at $4e(0,0,z)$ and C at $2b(0,0,1/2)$, where z is the so-called internal parameter. Thus, this structure is defined by two lattice parameters (a and c) and one internal parameter (z). Like other high-T_c superconductors, the body-centered-tetragonal structure of these superconductors can be resolved into atomic layers with square mesh. The stowing along the c axis is the sequence B-M_2-B-RC. The $(M\text{B})_2$ layers include a square-planar M_2 array sandwiched between the B planes with M atoms being tetrahedrally bonded to four neighboring B atoms. Thus, there are $M\text{B}_4$ tetrahedra, with a B-M-B bond angle of $\alpha_{\text{B-}M\text{-B}}$.

To determine the ground-state properties, the total energy is calculated as a function of volume and fitted to the Murnaghan equation of state [80]. The calculated equilibrium lattice constants (a and c), the equilibrium volume (V), the internal parameter z, the closest M-M separation ($d_{M\text{-}M}$), the closest B-C separation ($d_{\text{B-C}}$), the closest M-B separation ($d_{M\text{-B}}$), the B-M-B bond angle ($\alpha_{\text{B-}M\text{-B}}$), the bulk modulus ($B$), and its pressure derivative (B′) are presented and compared with available experimental [12–14,16,21–23,25,31] and theoretical results [58,59] in Table I. The calculated equilibrium volumes of these compounds deviate from their experimental values [12–14,16,21–23,25,31] by around 2.5%, while the calculated internal parameters z for $LaPt_2B_2C$ and $LuNi_2B_2C$ are almost equal to their experimental values [12]. This level of disagreement in the lattice constants, and thus the equilibrium volume, is quite common for theories based on the generalized gradient approximation. Unfortunately, there are no previous experimental and theoretical results to compare our GGA results for B and B′. The calculated volume and bulk modulus values for YPd_2B_2C and $LuNi_2B_2C$ are smaller than their LDA values [58,59]. The closest Pt-Pt separation is found to be 2.76 and 2.69 Å for $LaPt_2B_2C$ and YPt_2B_2C, respectively. These two values are smaller than the corresponding value of 2.78 Å in the fcc metal Pt. This result shows strong Pt-Pt metallic bonding in these compounds. A similar observation can be

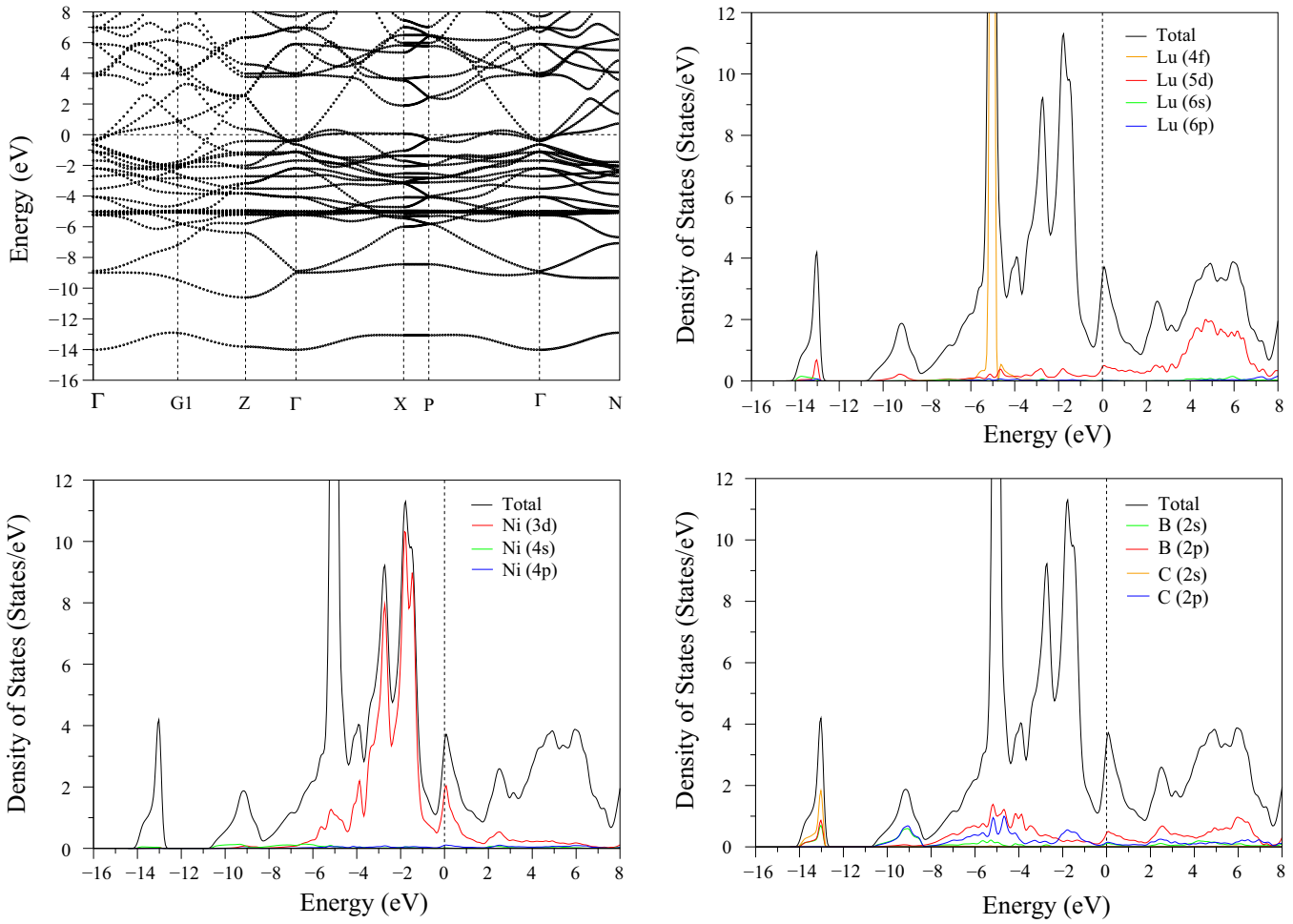

FIG. 2. (Color online) The electronic band structure and electronic density of states for the body-centered-tetragonal $LuNi_2B_2C$. The Fermi level is fixed to 0 eV. The high-symmetry points in the irreducible Brillouin zone in Cartesian coordinates are $G1 = \frac{2\pi}{a}((\frac{1}{2} + \frac{a^2}{2c^2}),0.00,0.00)$, $Z = \frac{2\pi}{a}(0.00,0.00,\frac{a}{c})$, $X = \frac{2\pi}{a}(0.50,0.50,0.00)$, $P = \frac{2\pi}{a}(0.50,0.50,\frac{a}{2c})$, and $N = \frac{2\pi}{a}(0.0,0.50,\frac{a}{2c})$. Note that $G1$ is the zone boundary in the [100] direction.

made for YPd_2B_2C and $LuNi_2B_2C$ compounds. There is a significant amount of covalent bonding in three dimensions, in particular between the transition metal and boron, and between boron and carbon atoms. As can be seen from Table I, the R-size difference does not change the value of the bond-length between B and C atoms. Finally, the calculated values of $\alpha_{\text{B-}M\text{-B}}$ for $LaPt_2B_2C$ and $LuNi_2B_2C$ accord very well with their experimental values [12] of 106.09° and 107.80°.

The electronic structure and electronic density of states for $LuNi_2B_2C$ are shown in Fig. 2. The overall band profiles are found to be in good agreement with previous theoretical calculations [52–55]. The low-lying C $2s$ band, with the maximal dispersion of ∼1.0 eV, is separated from the next band group by a gap of about 2.2 eV. Crossing a pseudogap, the hybridized B $2s$ and C $2p$ states are located between −10.7 and −7.0 eV below the Fermi level, which confirms the s-p bonding between B and C. The flat bands around −5.0 eV are due to Lu $4f$ states, which weakly hybridize with the other valence-band states. From −5.0 eV to the Fermi level, the formation of the valence bands comes from the combination of Ni $3d$, B $2p$, C $2p$, and Lu $5d$ states, with the maximum contribution coming from Ni $3d$ states. The energy bands close to the Fermi level show considerable dispersion along the Γ-Z direction, confirming the three-dimensional electronic structure of $LuNi_2B_2C$. A striking feature in the electronic structure of this material is the existence of an almost flat band along the Γ-X and Γ-P symmetry directions near the Fermi level, which causes a peak in the density of states. The Fermi level lies on this peak with an energy of 0.08 eV and is mainly made up of Ni $3d$ states with some contributions coming from Lu $5d$, B $2p$, and C $2p$ states. Thus, the metallic properties of $LuNi_2B_2C$ are characterized by the d states coming from the transition-metal Ni atoms. The value of the DOS at the Fermi level [$N(E_F)$] amounts to 3.64 states/eV, which is in good accordance with the previous theoretical value of 3.88 states/eV in the LDA study of Kim *et al.* [57]. The contributions of Lu, Ni, B, and C atoms to $N(E_F)$ are approximately 15%, 62%, 18%, and 5%, respectively. The contributions of Lu $5d$, Ni $3d$, B $2p$, and C $2p$ to $N(E_F)$ are 14%, 60%, 14%, and 4% to $N(E_F)$, respectively.

The electronic structures and electronic density of states for $LaPt_2B_2C$ and YPt_2B_2C are illustrated in Fig. 3. The electronic structure of these materials is substantially similar to that of $LuNi_2B_2C$, except that the nearly flat band along Γ-X lies

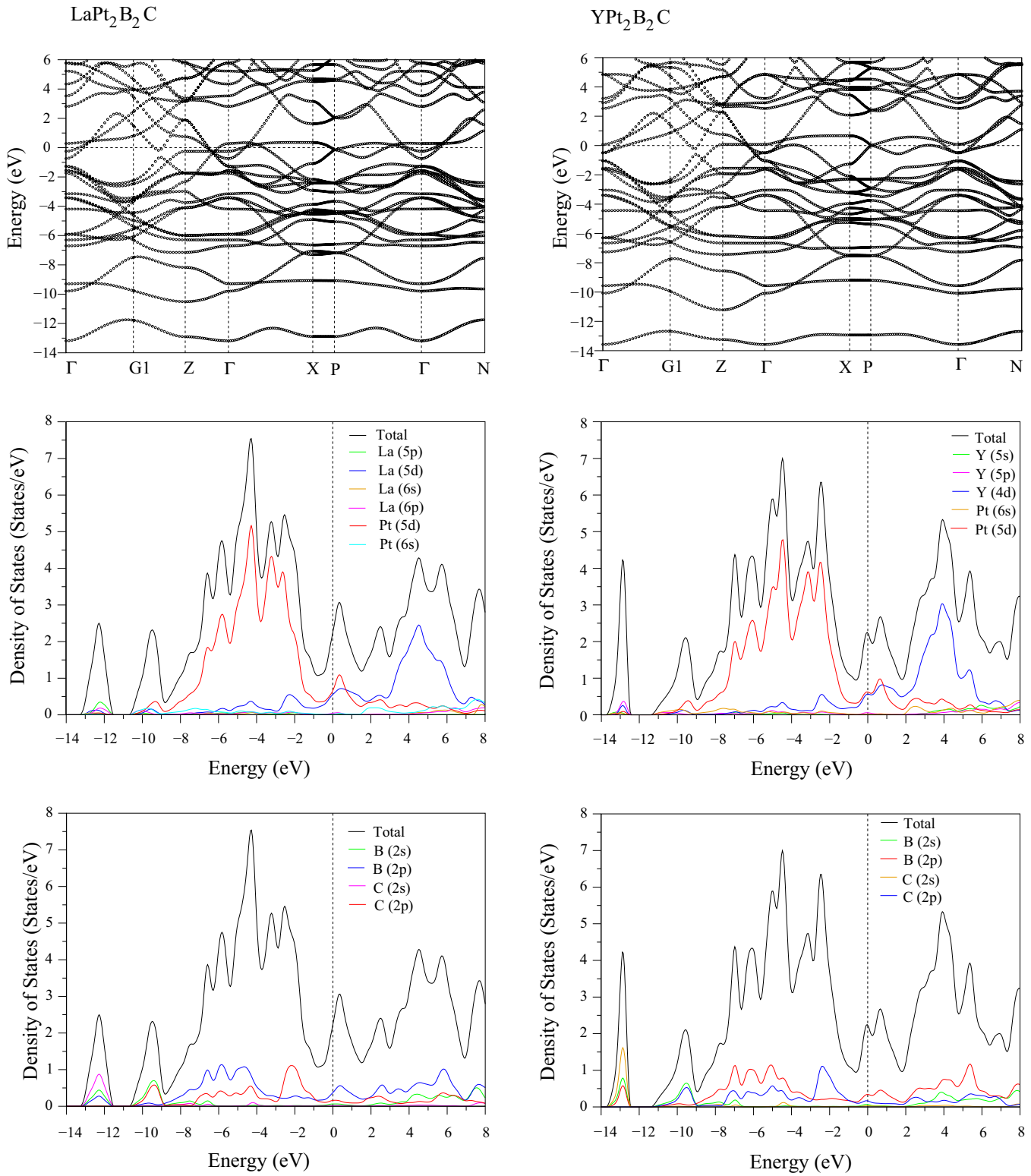

FIG. 3. (Color online) The electronic band structure and electronic density of states for the body-centered-tetragonal $LaPt_2B_2C$ and YPt_2B_2C. The Fermi level is fixed to 0 eV.

somewhat higher than the Fermi energy. A characteristic of the borocarbide superconductors is the existence of a nearly flat band along the Γ-X direction. The main valence band for both materials is dominated by the contributions of all the atoms in both compounds. Different from $LuNi_2B_2C$, the contributions of $R\,d$, B $2p$ and C $2p$ states to the main valence-band region in these compounds are greater than those in $LuNi_2B_2C$. Secondly, the transition-metal bandwidth in these materials is larger than that in $LuNi_2B_2C$ due to the replacement of the $3d$ Ni atom by the $5d$ Pt atom. Because

TABLE II. The zone-center phonon modes (in THz) of RM_2B_2C superconductors and their comparison with previous experimental and theoretical results.

Material	E_u	A_{2u}	B_{1g}	E_g	E_u	A_{2u}	E_u	E_g	A_{1g}	A_{2u}
$LuNi_2B_2C$										
Present GGA work	3.44	3.95	6.04	9.01	12.26	12.58	13.42	13.54	24.96	38.64
LDA [54]									25.48	
LDA [58]			5.97						26.77	
GGA [60]	3.45	3.36	5.64	8.99	11.96	12.29	13.42	13.82	26.05	38.67
Raman [50]			5.70						25.87	
YPd_2B_2C	2.72	4.05	2.55	7.30	8.87	10.54	10.58	11.64	26.04	40.78
YPt_2B_2C										
Present GGA work	2.87	3.82	1.68	6.23	8.75	11.00	12.15	12.06	27.67	40.56
$LaPt_2B_2C$										
Present GGA work	2.87	3.95	1.96	5.46	8.74	10.40	12.39	11.70	26.15	38.71

the DOS distribution near the Fermi level (E_F) plays an important role in determining superconducting properties, it is imperative to analyze the DOS in the vicinity of the Fermi level for both materials. The Fermi level for $LaPt_2B_2C$ lies on a sharply increasing peak at 0.40 eV. This peak is formed by the nearly equal contributions of La $5d$ and Pt states, with some contributions coming from B $2p$ and C $2p$ states. However, the similar peak at 0.08 eV for $LuNi_2B_2C$ is mainly dominated by transition-metal d states. The numerical value of the DOS at the Fermi level [$N(E_F)$] is 2.18 states/eV for $LaPt_2B_2C$, which is lower than the corresponding value of 3.64 states/eV for $LuNi_2B_2C$. The contribution of La, Pt, B, and C atoms to $N(E_F)$ is 30%, 36%, 23%, and 11%, respectively. This result indicates that the R atoms in $LaPt_2B_2C$ make a considerably larger contribution to $N(E_F)$ than the R atoms in $LuNi_2B_2C$. Moreover, the contributions from B and C atoms to $N(E_F)$ for $LaPt_2B_2C$ are also considerably increased. The value of $N(E_F)$ amounts to 1.96 states/eV for YPt_2B_2C, which is also smaller than that for $LuNi_2B_2C$. For this material, Y and Pt d states make a nearly equal contribution to $N(E_F)$ while the contribution of B and C atoms to $N(E_F)$ is 21% and 12%. Again, the contribution of transition-metal atoms to $N(E_F)$ is significantly decreased compared to that in $LuNi_2B_2C$. The electronic properties of YPd_2B_2C are clearly presented and discussed in our previous *ab initio* work [62]. Thus, we will not repeat them here. The $N(E_F)$ value for this superconductor is 2.64 states/eV. The difference in their $N(E_F)$ values will certainly affect the superconducting properties of these materials, since according to the McMillan-Hopfield expression, the electron-phonon coupling constant (λ) can be given in the following form [72,73]:

$$\lambda = \frac{N(E_F)\langle I^2\rangle}{M\langle\omega^2\rangle}, \tag{5}$$

where M represents the average atomic mass and $\langle\omega^2\rangle$ denotes the average of squared phonon frequencies. Further, $\langle I^2\rangle$ represents the Fermi surface average of the squared electron-phonon coupling interaction. The above equation shows that the electron-phonon coupling constant increases linearly with $N(E_F)$.

B. Phonons and electron-phonon interaction

The zone-center phonon modes for RM_2B_2C can be categorized by the irreducible representation of the point group D_{4h} $(4/mmm)$. As determined from group theory, the symmetries of the optical-phonon modes are given as

$$\Gamma = E_u^1 + A_{2u}^1 + B_{1g} + E_g^1 + E_u^2 + A_{2u}^2 + E_u^3 + E_g^2 + A_{1g} + A_{2u}^3,$$

where the E modes are doubly degenerate. There are a total of eight Raman-active vibrational modes ($B_{1g} + E_u^1 + E_g^1 + E_g^2 + A_{1g}$) and seven infrared-active vibrational modes ($A_{2u}^1 + E_u^2 + A_{2u}^2 + E_u^3 + A_{2u}^3$). We have identified the symmetries of these modes using their eigenvectors, and they are presented in Table II. In particular, the calculated zone-center phonon frequencies for $LuNi_2B_2C$ are compared with previous theoretical [54,58,60] and experimental results [50] in this table. It can be seen that the calculated frequencies for $LuNi_2B_2C$ are in good accordance with previous theoretical results [54,58,60] while the calculated frequencies of the B_{1g} and A_{1g} phonon modes compare well with their Raman values within 6%. The eigenvectors of these phonon modes show that the double E modes are dominated by the vibrations of atoms along the $\hat{x}$ and $\hat{y}$ axes, whereas the A and B modes result from the vibrations of atoms along the $\hat{z}$ axis.

TABLE III. The calculated zone-center electron-phonon coupling parameters for RM_2B_2C superconductors.

Material	E_u	A_{2u}	B_{1g}	E_g	E_u	A_{2u}	E_u	E_g	A_{1g}	A_{2u}
$LuNi_2B_2C$	0.008	0.006	0.108	0.021	0.010	0.000	0.015	0.020	0.336	0.000
YPd_2B_2C	0.047	0.007	0.246	0.014	0.032	0.000	0.049	0.028	0.225	0.001
YPt_2B_2C	0.015	0.003	0.296	0.011	0.018	0.000	0.012	0.013	0.109	0.000
$LaPt_2B_2C$	0.003	0.001	0.646	0.053	0.015	0.000	0.015	0.049	0.375	0.000

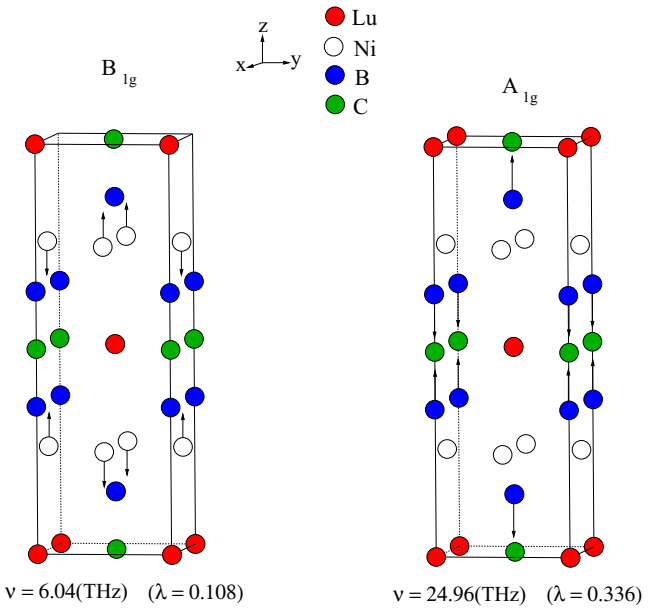

FIG. 4. (Color online) Eigenvector representations of the zone-center B_{1g} and A_{1g} phonon modes in the body-centered-tetragonal $LuNi_2B_2C$.

The electron-phonon coupling parameters of zone-center optical-phonon modes for RM_2B_2C are listed in Table III. Our calculations indicate that all zone-center optical-phonon modes have a negligibly small electron-phonon coupling parameter except for the B_{1g} and A_{1g} phonon modes. The eigenvector representations of these phonon modes for $LuNi_2B_2C$ are shown in Fig. 4. The eigenvector representation of the B_{1g} phonon mode dynamically changes the tetrahedral bond angles in NiB_4, which causes the overlap of Ni and B electronic states. This overlap leads to a larger electron-phonon coupling parameter for the B_{1g} phonon mode than other zone-center phonon modes. The eigenvector representation of the A_{1g} phonon mode stretches or compresses the B-C bonds, which lead to the overlap of B and C electronic states. The electron-phonon coupling parameter of the A_{1g} phonon mode for RM_2B_2C decreases rapidly with increasing $\boldsymbol{q}$ wave vector. This feature can be seen clearly in Fig. 5. A similar observation has been made for YNi_2B_2C in the theoretical work of Reichardt *et al.* [61].

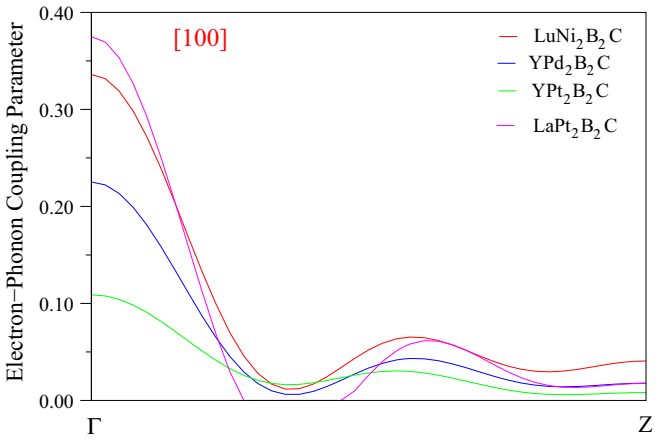

FIG. 5. (Color online) The calculated wave-vector-dependent electron-phonon coupling parameter of A_{1g} phonon mode for RM_2B_2C along the [100] symmetry direction.

In agreement with previous theoretical studies [53,54], the largest electron-phonon coupling parameter (λ) is found for the A_{1g} phonon mode of $LuNi_2B_2C$ with a value of 0.336. However, one of the previous theoretical works [54] suggested that the value of the electron-phonon coupling parameter (λ) for this phonon mode is between 1.0 and 2.0. Due to this observation, previous theoretical works [53,54] conclude that the zone-center A_{1g} phonon mode and its strong coupling with electrons are essential for the superconductivity in $LuNi_2B_2C$. Our calculations clearly show that this conclusion is wrong, because the strength of the electron-phonon interaction for this phonon mode is weak ($\lambda^{A_{1g}} < 0.5$) rather than strong. This low electron-phonon coupling parameter cannot produce the superconducting transition temperature of around 16 K. Thus, we can conclude that the contributions of phonon modes away from the zone center to the electron-phonon coupling parameter must be calculated and discussed. We will do this after presenting phonon-dispersion curves for all the studied compounds. Our present and previous works [62] confirm clearly that phonon-dispersion curves should be calculated for a full analysis of electron-phonon interaction in any BCS-type superconductor.

The left panels in Fig. 6 show the calculated phonon spectrum of $LuNi_2B_2C$ along the various high-symmetry directions in the IBZ. The frequency spectrum of all of the 18 phonon branches can be divided into three obvious regions: a low-frequency region (LFR) between 0 and 9.3 THz, an intermediate-frequency region (IFR) between 10.3 and 15.6 THz, and a high-frequency region (HFR) above 24.5 THz. There are three acoustic- and six optical-phonon branches in the LFR, all exhibiting highly dispersive behavior. A gap of around 1.0 THz exists between the LFR and IFR, due to the mass difference between the different types of atoms in the unit cell. The IFR contains seven optical-phonon modes that exhibit a considerable amount of dispersion. The top two phonon branches lie in the HFR, which is separated from the IFR by a huge optical-optical gap of 9 THz. These two phonon branches exhibit very little dispersion compared to the branches in the other two regions.

The total and partial phonon density of states (pDOS) are shown in the right panels in Fig. 6. Based on our analysis of the eigenvectors for each atom in the unit cell, we have observed that the first region, particularly below 4.4 THz, is mainly contributed by the vibrations of the heaviest Lu atoms, with some contribution coming from the vibrations of the remaining atoms. The frequency region from 4.4 to 7 THz is dominated by the vibrations of Ni atoms with smaller contributions coming from B and C atoms. The frequency region from 7.0 to 9.3 THz arises from the coupled motion of Ni and B atoms. Although B atoms are the lightest of the four types of atoms, they make a considerable contribution to phonon branches in the LFR. This observation indicates the presence of a strong covalent bonding force between Ni and B atoms. The pDOS shows a dominance of B atoms in the frequency region between 10.3 and 13.6 THz, with a smaller admixture of C atoms. The partial pDOS illustrates a dominance of C

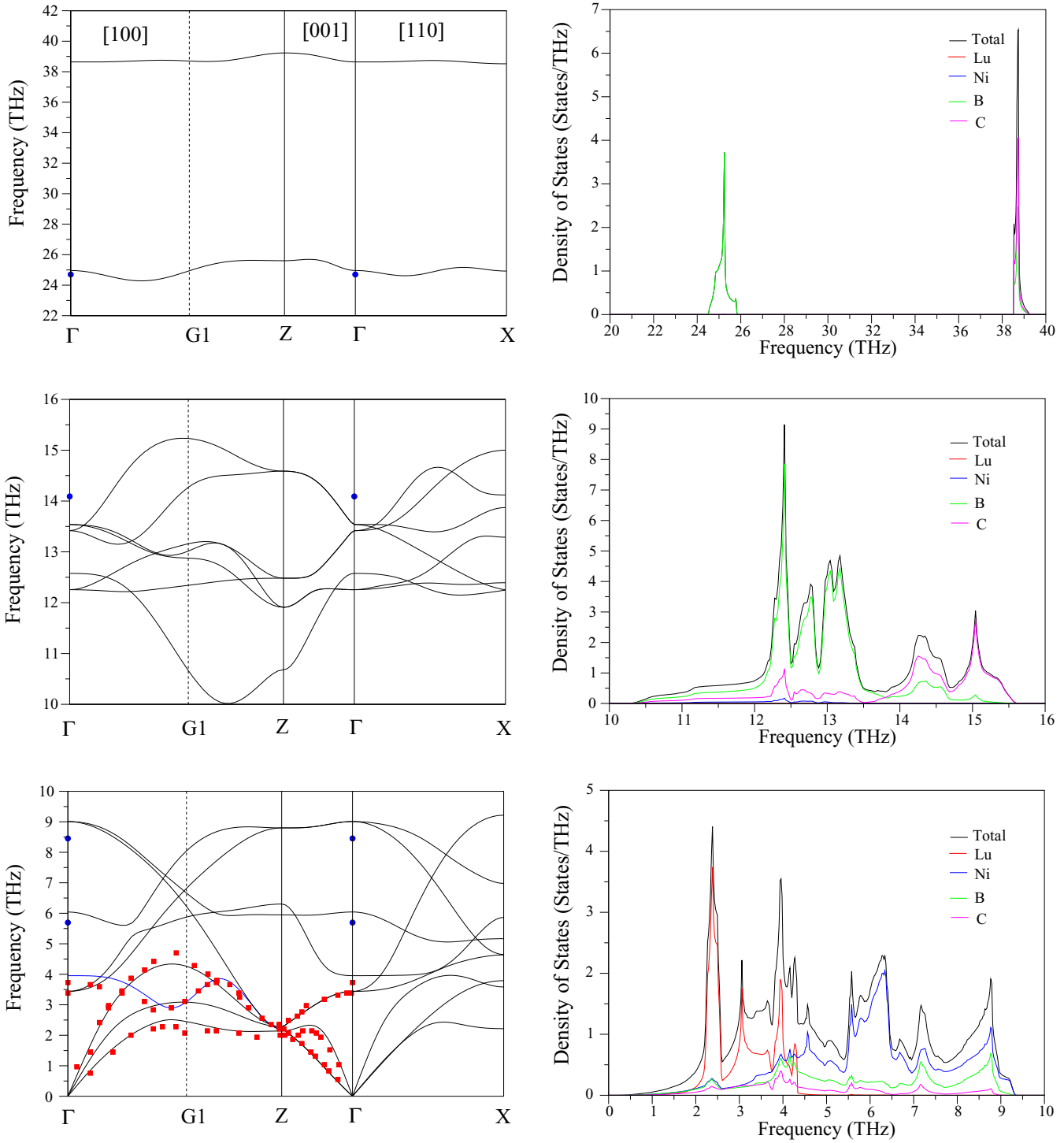

FIG. 6. (Color online) Phonon-dispersion curves and density of states for $LuNi_2B_2C$. The anomaly of the A_{2u} phonon branch is shown by the blue solid line. Inelastic-neutron-scattering results [49] and Raman results are shown by red squares and blue circles [50], respectively.

atoms with considerable contributions coming from B atoms in the frequency region between 13.6 and 15.6 THz. There is a large gap of 14 THz separating the two upper sharp peaks at 25.4 and 39.3 THz. The contribution of B atoms to the peak at around 25.4 THz is the strongest. The highest-frequency band at around 39.3 THz has an almost pure B-C bond-stretching character, confirming the strong covalent bond between B and C atoms.

An important feature of the phonon spectrum for $LuNi_2B_2C$ is the softening of the A_{2u} optical branch along the Γ-$G1$-Z ([100]) symmetry direction. Along this direction, this branch acquires a "dip," with frequency lower than the second transverse-acoustic (TA) branch. This remarkable phonon anomaly of the A_{2u} branch seems to be very important in the superconductivity of $LuNi_2B_2C$, as previous theoretical studies on transition-carbide superconductors such as NbC,

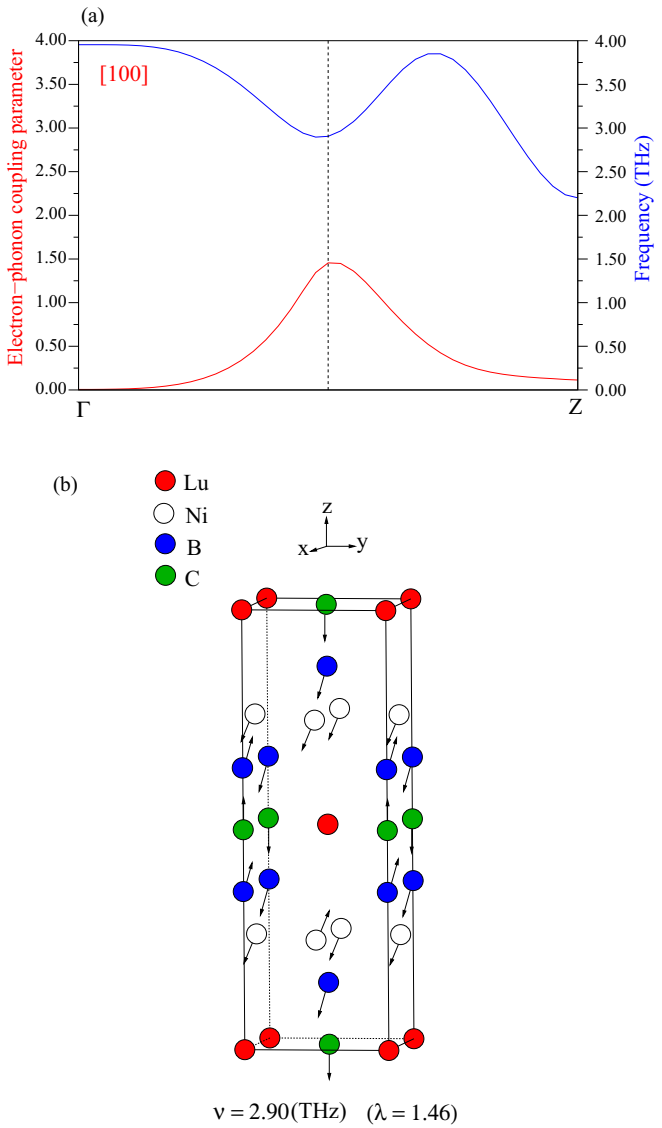

FIG. 7. (Color online) (a) The electron-phonon coupling parameter (red line) and frequency (blue line) of the A_{2u} phonon branch along the [100] direction in $LuNi_2B_2C$. The dashed line indicates $\mathbf{q} = \frac{2.\pi}{a}(0.50,0.00,0.00)$. (b) A schematic illustration of the eigendisplacement pattern of the A_{2u} phonon mode (2.90 THz) at $\mathbf{q} = \frac{2.\pi}{a}(0.50,0.00,0.00)$.

TaC, and CrC [81–83] have indicated that a strong phonon anomaly gives rise to a large electron-phonon coupling parameter. To correlate the anomalous phonon dispersion of A_{2u} with electron-phonon interaction, we display together the frequency-dependent electron-phonon coupling parameter $\lambda(\omega)$ and the frequency dispersion of this phonon mode in Fig. 7(a). Clearly, the most notable feature is that the electron-phonon coupling parameter of the A_{2u} branch reaches a peak value of 1.46 at $\boldsymbol{q} = \frac{2.\pi}{a}(0.50,0.00,0.00)$, where the frequency of this branch takes its lowest value of 2.90 THz. Thus, this observation confirms a positive relationship between phonon anomaly and electron-phonon coupling parameter. Figure 7(b) shows a schematic illustration of the eigendisplacement pattern of the A_{2u} phonon branch at $\boldsymbol{q} = \frac{2.\pi}{a}(0.50,0.00,0.00)$. This vibrational pattern stretches the B-C bonds and modulates the tetrahedral B-Ni-B bond angles at the same time. This phonon mode includes large atomic displacements from Ni atoms. This is expected because the states near the Fermi energy are mainly dominated by Ni d orbitals. Thus, this displacement pattern causes big changes in the overlap of electronic orbitals between neighboring atoms, leading to a large electron-phonon coupling parameter. Previous theoretical studies [54,58,60] could not make this observation since they only calculated the zone-center phonon modes in $LuNi_2B_2C$.

The calculated phonon-dispersion relations and the phonon density of states for YPd_2B_2C are displayed in Fig. 8. Different from the phonon spectrum of $LuNi_2B_2C$, the phonon-dispersion curves for YPd_2B_2C can be divided into two clear regions: a low-frequency region between 0 and 13.2 THz and a high-frequency region above 25.5 THz. A large gap of about 12.0 THz between these regions comes from the mass difference between the different types of atoms in the unit cell. There are three acoustic and thirteen optical bands extending up to 13.2 THz in the low-frequency region, and all phonon branches in this region show a considerable amount of dispersion. In the upper frequency range, there are two nearly flat phonon bands. The calculated pDOS for YPd_2B_2C shows that the low-frequency region below 4.3 THz consists of the acoustical and optical vibrations of Y and Pd atoms with some contributions coming from B and C atoms. The frequency region from 4.3 to 8.9 THz arises from the coupled motion of B, C, and Y atoms, with Pd atoms at rest. The partial pDOS shows a strong B-C hybridization in the frequency range from 8.9 to 13.2 THz, and a negligible contribution from Y and Pd atoms. The peak at 25.9 THz is totally dominated by the vibrations of B atoms, while the highest peak at 40.6 THz originates from the coupled motion of B and C atoms. The most obtrusive feature of the phonon spectrum for YPd_2B_2C is the anomalous behavior exhibited by the first transverse-acoustic branch (TA_1) along the [100] direction. As a result of this phonon anomaly, the electron-phonon coupling parameter of this branch hardens rapidly with increasing wave vector up to $\boldsymbol{q} = \frac{2\pi}{a}(0.55,\ 0.00,\ 0.00)$, which can be seen from Fig. 9(a). The electron-phonon coupling parameter of this branch branch reaches a peak value of 4.12 at this $\boldsymbol{q}$ point, while its phonon frequency exhibits a dip value of 1.18 THz. This observation is also clear evidence of a positive relationship between the phonon anomaly and the electron-phonon coupling parameter. Figure 9(b) displays a schematic illustration of the eigendisplacement pattern of the TA_1 phonon branch at $\boldsymbol{q} = \frac{2.\pi}{a}(0.55,0.00,0.00)$. This vibrational pattern also causes significant changes to the B-C bonds and the tetrahedral B-Pd-B bond angles at the same time.

The calculated phonon-dispersion relations and the phonon density of states for $LaPt_2B_2C$ are illustrated in Fig. 10. Different from $LuNi_2B_2C$, we could not observe any phonon anomaly in the phonon spectrum of $LaPt_2B_2C$ before the zone boundary of $G1$ along the [100] direction (see Fig. 10). Three acoustic- and six optical-phonon branches form a low-frequency region below 5.8 THz, while the intermediate-frequency region from 7.3 to 13.8 THz is generated by seven dispersive optical-phonon branches. These two regions are separated from each other by a gap of 1.5 THz. Phonon modes in these regions lie in lower frequencies than the corresponding phonon modes in $LuNi_2B_2C$ due to the larger unit-cell volume

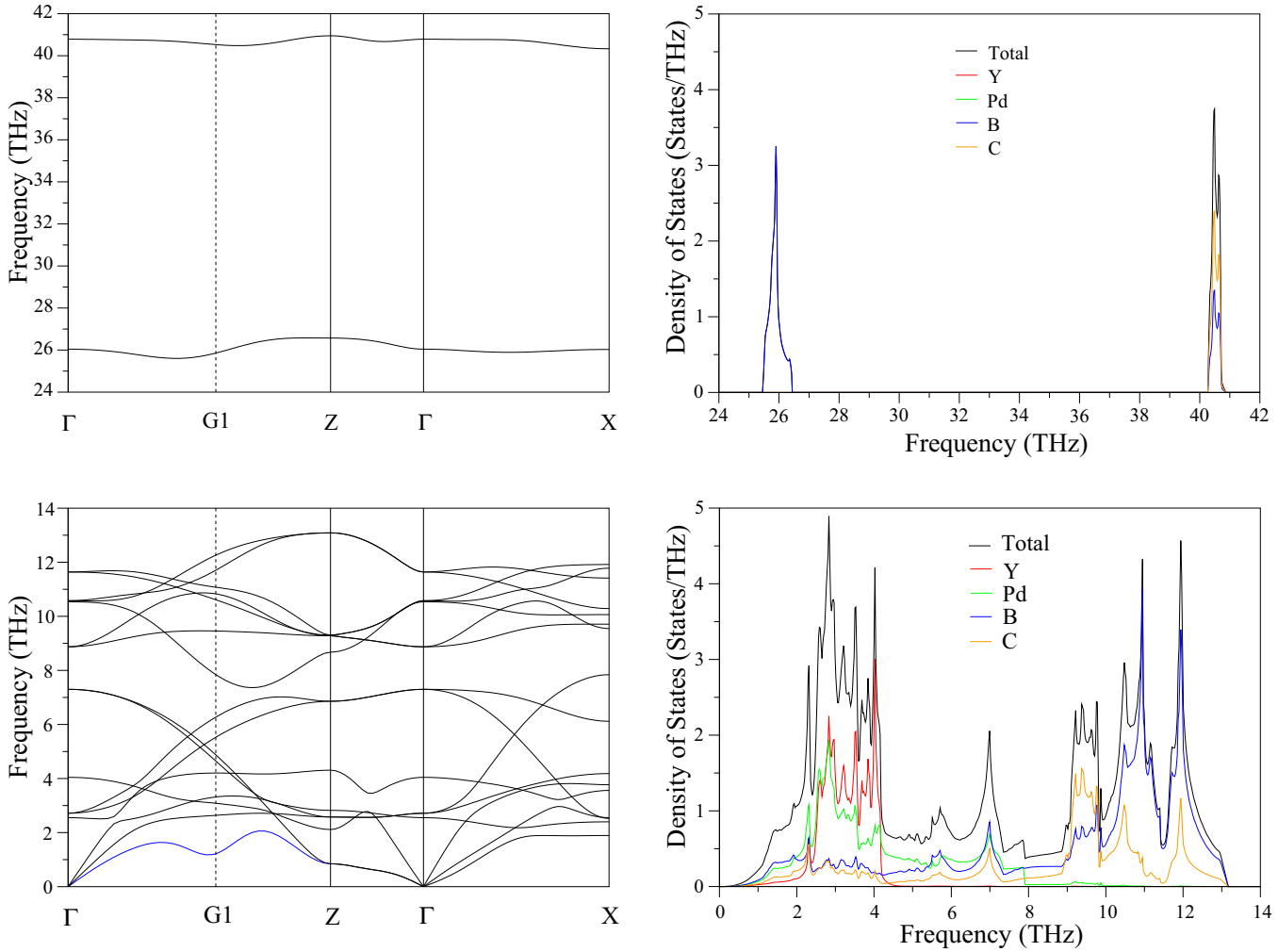

FIG. 8. (Color online) Phonon-dispersion curves and density of states for YPd_2B_2C. The anomaly of the first transverse-acoustic branch (TA_1) is shown by the blue line.

of $LaPt_2B_2C$ as compared to that of $LuNi_2B_2C$. Moreover, the mass of a Pt atom is much heavier than that of an Ni atom. In agreement with $LuNi_2B_2C$ and YPd_2B_2C, two nearly dispersionless phonon bands exist in the high-frequency region above 24 THz. From the phonon density of states for $LaPt_2B_2C$, we have found that while Pt, as the heaviest element, dominates the lower frequencies in the range of 0–2.5 THz, a strong La-Pt hybridization is observed in the range of 2.5–4.0 THz. Some contributions from B and C atoms to the DOS have been seen below 4.0 THz. The main contribution to the DOS from 7.3 to 12.2 THz comes from B vibrational modes with some contribution from C atoms. In the range of 12.4-13.8 THz, a very strong B-C hybridization can be seen due to the small mass difference between these atoms. Finally, the sharp peaks at 25.3 and 38.7 THz have similar characters to the corresponding peaks in $LuNi_2B_2C$ and YPd_2B_2C.

The calculated phonon-dispersion relations and the phonon density of states for YPt_2B_2C are displayed in Fig. 11. In general, the phonon spectrum of this compound looks roughly similar to that of $LaPt_2B_2C$, except for two differences. First, in agreement with YPd_2B_2C, a phonon anomaly has been observed for the TA_1 branch of this material near the zone boundary $G1$ along the [100] direction (see the blue line in Fig. 11). However, this anomaly is not as strong as that in the phonon spectrum of YPd_2B_2C (see Fig. 8). Thus, relating the phonon anomaly to the strength of the electron-phonon interaction, we can state that the latter should be much weaker in YPt_2B_2 than in YPd_2B_2C. Secondly, the A_{2u} phonon branch in YPt_2B_2C (see the green line in Fig. 11) along the Γ-Z direction is softer than the corresponding branch in $LaPt_2B_2C$. Thirdly, the B_{1g} phonon branch in YPt_2B_2C (see the red line in Fig. 11) along the Γ-X direction is much softer than the corresponding branch in $LaPt_2B_2C$. This observation indicates that the electron-phonon interaction should be slightly stronger in YPt_2B_2C than that in $LaPt_2B_2C$. To see the contributions of these three phonon branches to the electron-phonon interaction in YPt_2B_2C, we have plotted their contributions to the electron-phonon coupling parameter in Fig. 12. This figure confirms the above statements, viz. that the softening of the TA_1 and A_{2u} and B_{1g} phonon branches causes a large electron-phonon interaction in YPt_2B_2C.

To find the strengths with which different vibrational modes couple to electrons, and thus affect the superconducting

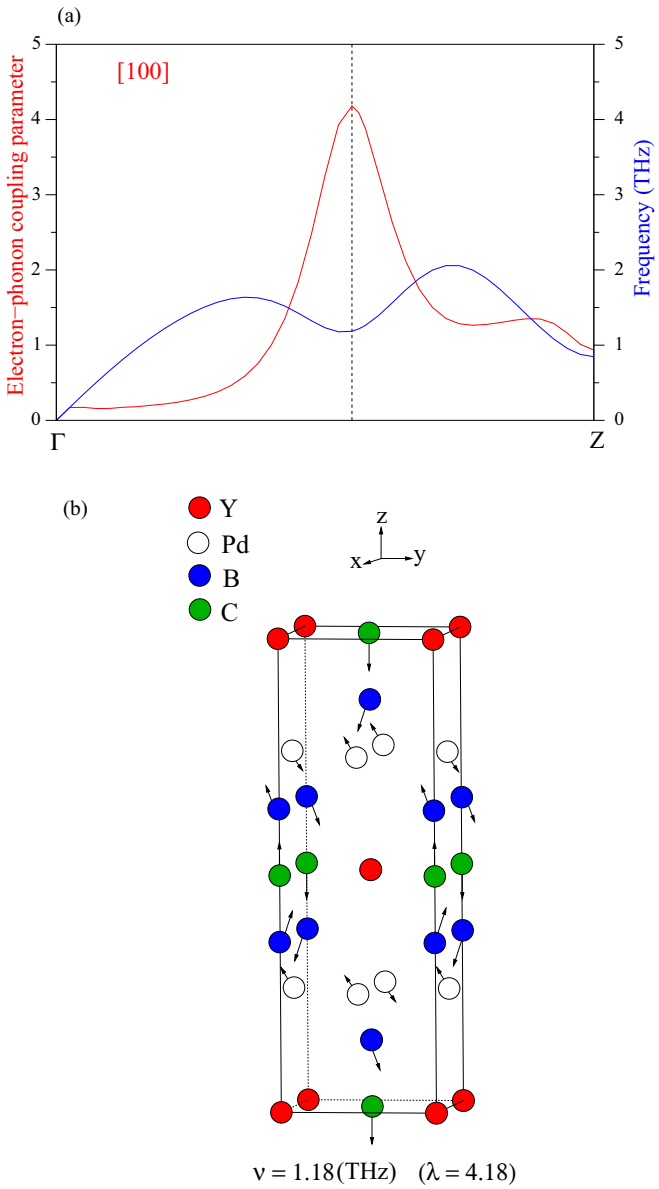

FIG. 9. (Color online) (a) The wave-vector-dependent electron-phonon coupling parameter (red line) and frequency (blue line) of the first transverse-acoustic branch (TA_1) along the [100] direction in YPd_2B_2C. The dashed indicates $\mathbf{q} = \frac{2.\pi}{a}(0.55,0.00,0.00)$. (b) A schematic illustration of the eigendisplacement pattern of the TA_1 phonon mode at $\mathbf{q} = \frac{2.\pi}{a}(0.55,0.00,0.00)$.

properties, the Eliashberg spectral function $[\alpha^2 F(\omega)]$ is calculated for all the materials studied here. Figure 13 shows the variation of the Eliashberg spectral function $\alpha^2 F(\omega)$ and the cumulative frequency variation of the electron-phonon coupling parameter λ_ω,

$$\lambda_\omega = 2\int_0^\omega \frac{\alpha^2 F(\omega')}{\omega'} d\omega' \quad (6)$$

$$= \int_0^\omega \lambda(\omega') d\omega'. \quad (7)$$

The numerical results for λ_ω are 0.78, 0.83, 0.96, and 1.48 for $LaPt_2B_2C$, $LuNi_2B_2C$, YPt_2B_2C, and YPd_2B_2C, respectively. Clearly, the cumulative electron-phonon coupling parameter is of strong strength for YPd_2B_2C. But the other three materials ($LaPt_2B_2C$, $LuNi_2B_2C$, and YPt_2B_2C) are characterized by an electron-phonon interaction of medium strength.

We now examine the spectral contribution to λ_ω for $LuNi_2B_2C$. In the frequency range from 0 to 9.5 THz, we find that λ increases rapidly with frequency. The phonon modes in this region contribute about 67% (0.56) to λ, while the contribution of phonon modes between 10.0 and 15.70 THz to λ is about 28% (0.23). Thus, we can state that acoustic as well as low-frequency optical-phonon branches make a huge contribution to the average electron-phonon coupling parameter. In particular, our results show that the A_{1g} phonon branch contributes about 4.7% to λ. This small contribution can be linked to the factor of $\frac{1}{\omega}$ in Eq. (7). This is in contrast to previous theoretical works [53,54], which suggest a strong electron-phonon interaction for the A_{1g} phonon mode of $LuNi_2B_2C$.

In general, a similar picture emerges for the other three materials. Thus, we can conclude that in addition to the A_{1g} phonon mode, acoustic phonon branches as well as low-frequency optical branches couple strongly with electrons to develop superconductivity in RM_2B_2C materials.

The electron-phonon coupling constant λ also enters the electronic specific-heat coefficient γ, which is renormalized by the "phonon enhancement" factor $(1+\lambda)$ compared to the "band-structure"value [74]:

$$\gamma_{\text{renorm}} = \gamma_{\text{bs}}(1+\lambda) = \tfrac{1}{3}\pi^2 k_B^2 N(E_F)(1+\lambda). \quad (8)$$

The superconducting transition temperature T_C can be calculated from the Allen-Dynes modified McMillian formula [72,73],

$$T_C = \frac{\omega_{\ln}}{1.2}\exp\left(-\frac{1.04(1+\lambda)}{\lambda-\mu^*(1+0.62\lambda)}\right), \quad (9)$$

$$\omega_{\ln} = \exp\left(2\lambda^{-1}\int_0^\infty \frac{d\omega}{\omega}\alpha^2 F(\omega)\ln\omega\right), \quad (10)$$

$$\Theta_D = \frac{1.45\omega_{\ln}}{1.2}, \quad (11)$$

where μ^* the effective screened Coulomb repulsion constant. The value of μ^* is taken to be 0.10 for all the RM_2B_2C compounds studied here. $\omega_{\ln}$ and Θ_D are the logarithmically averaged frequency and Debye frequency, respectively. The calculated values of $N(E_F)$, $\omega_{\ln}$, Θ_D, λ, γ, and T_c for RM_2B_2B are given in Table IV. Our results are also compared with available experimental and theoretical results in this table. In general, the calculated superconducting parameters for all studied materials are in acceptable agreement with their experimental values. In particular, the calculated λ value of 0.83 for $LuNi_2B_2C$ is in excellent accordance with its experimental value [7] of 0.80. As can be seen from the McMillan-Hopfield and the Allen-Dynes modified McMillian equations, the T_c values of BCS-type superconductors can be effected by three main factors: the density of states at the Fermi level $[N(E_F)]$, the logarithmic average phonon frequency $\omega_{\ln}$ (or the averaged square of the phonon frequency $\langle\omega^2\rangle$), and the strength of the electron-phonon coupling parameter λ. With

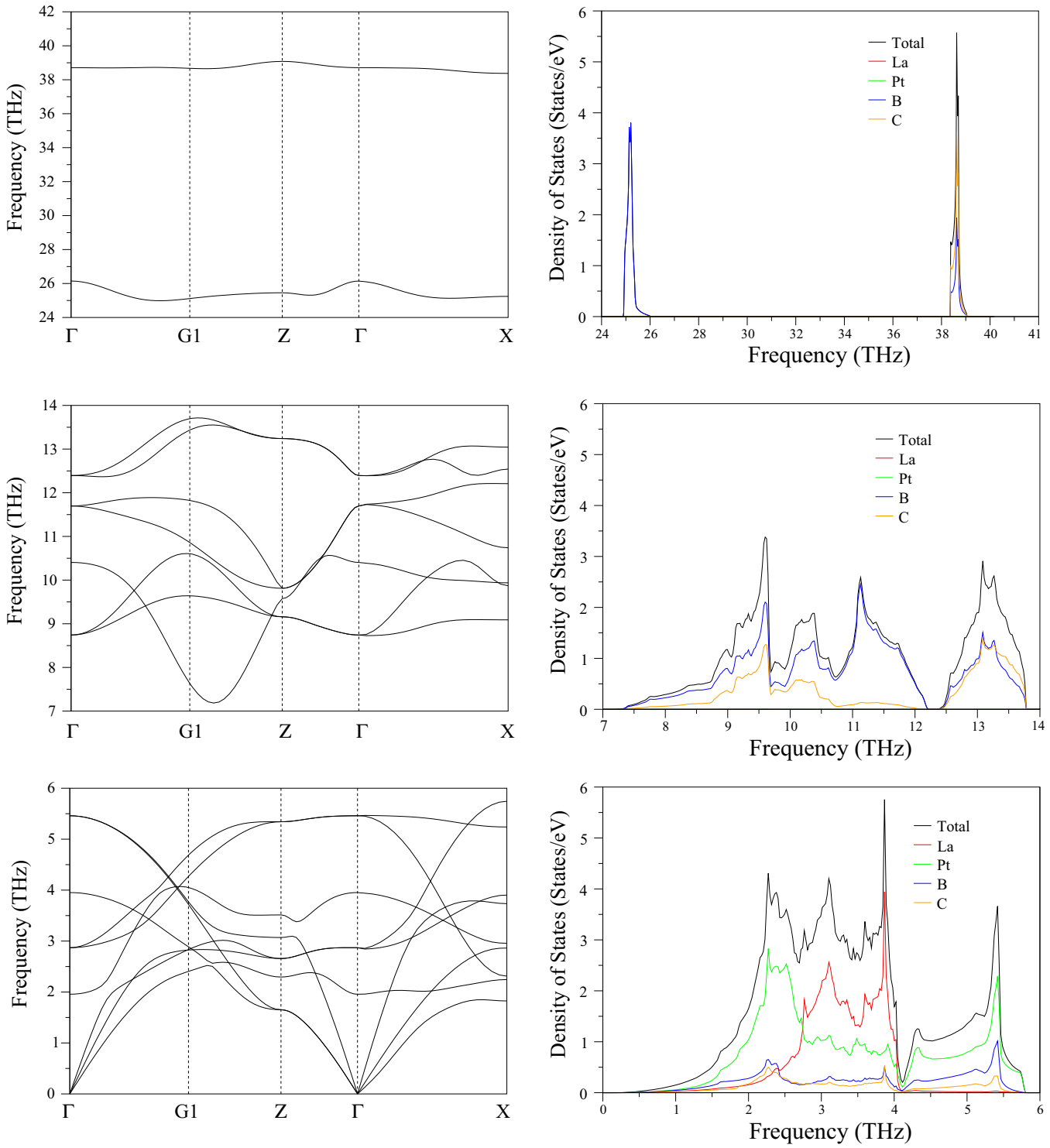

FIG. 10. (Color online) Phonon-dispersion curves and density of states for $LaPt_2B_2C$.

regard to the electronic structure, the largest $N(E_F)$ value is found for $LuNi_2B_2C$. However, the electron-phonon coupling parameter of this is smaller than the corresponding parameter for YPd_2B_2C and YPt_2B_2C. This can be related to the largest $\omega_{\ln}$ value of 315 K for $LuNi_2B_2C$ since the hardening of phonon frequencies makes a negative contribution to λ according to the McMillan-Hopfield expression. The largest T_c value of 20.6 K is found for YPd_2B_2C. We think that a strong phonon anomaly of the TA_1 branch is essential for this large value.

IV. SUMMARY

In this work, we have investigated the structural, electronic, vibrational, and superconducting properties of RM_2B_2C (R = Y,La,Lu and M = Ni,Pd,Pt) crystallizing in the

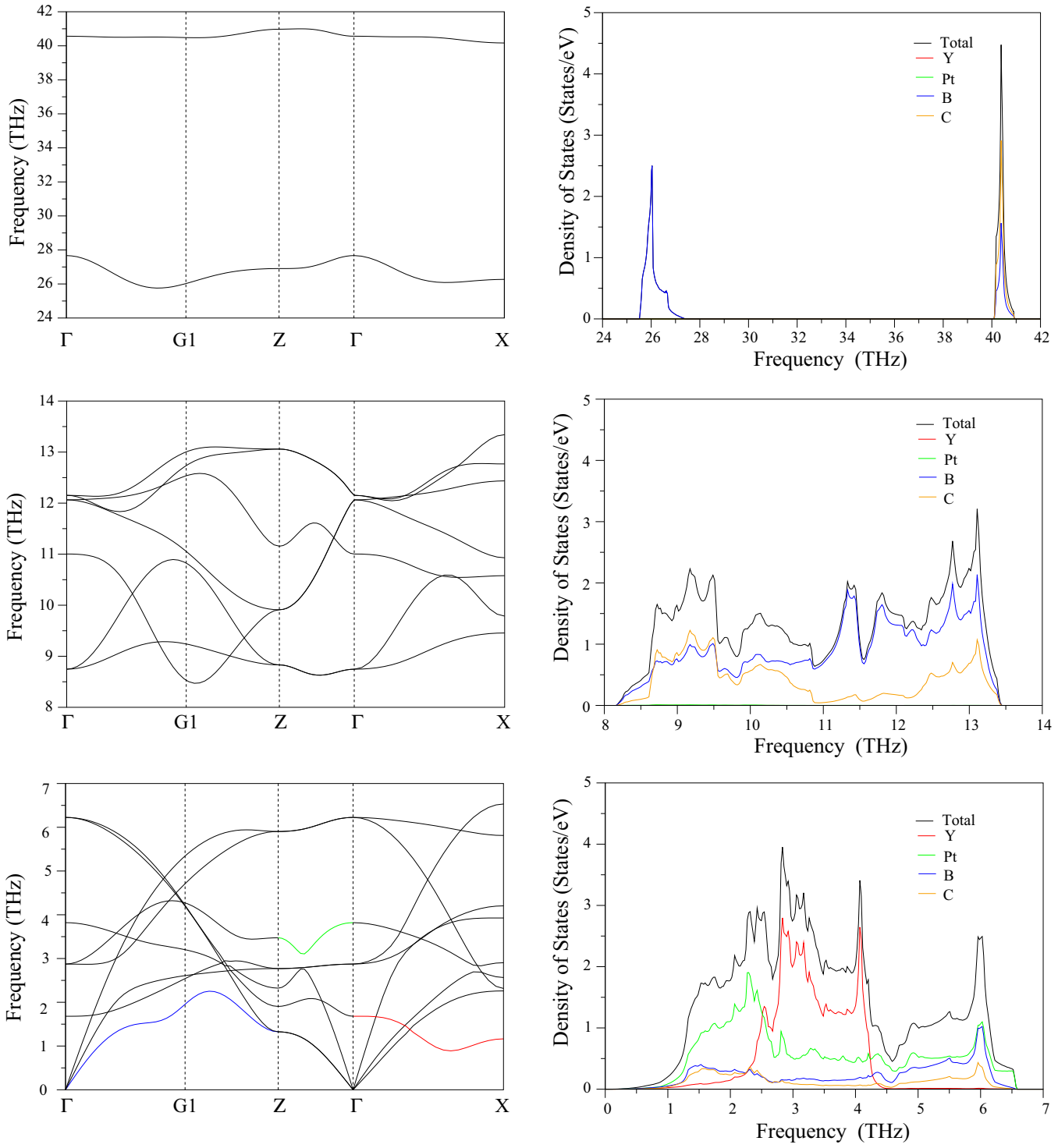

FIG. 11. (Color online) Phonon-dispersion curves and density of states for YPt_2B_2C. The anomalous dispersions of the TA_1, A_{2u}, and B_{1g} branches are shown by the blue, green solid, and red solid curves, respectively.

body-centered-tetragonal $LuNi_2B_2C$ type of crystal structure by using the generalized gradient approximation of the density-functional theory and the plane-wave pseudopotential method.

The obtained structural parameters for all studied materials compare very well with previous theoretical and experimental results. The calculated electronic structures of these borocarbides exhibit three-dimensional rather than two-dimensional characteristics because the energy bands are dispersive along the c axis. A main feature of the borocarbide family of superconductors is the subsistence of a nearly flat band, which creates a peak in their electronic density of states close to the Fermi level. The main valence-band complex is contributed by all types of atoms in the structure. However, the R contribution to $N(E_F)$ for $LuNi_2B_2C$ is smaller than the corresponding M

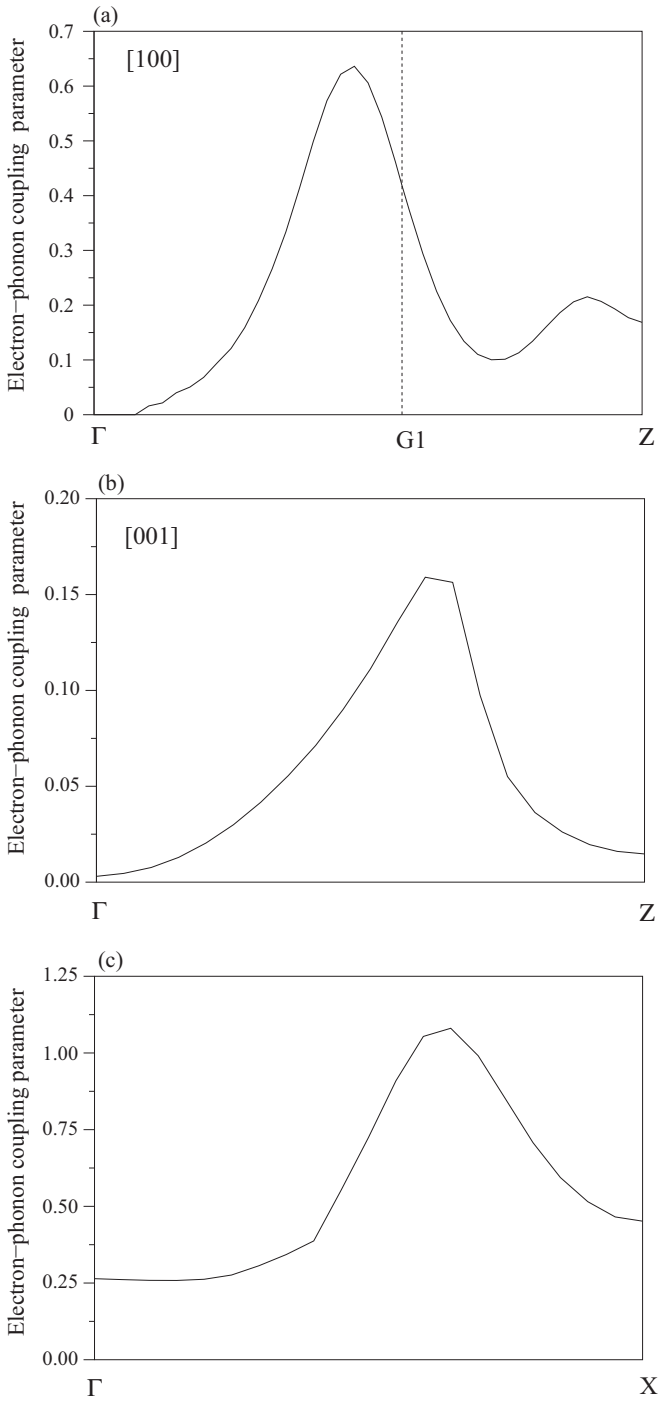

FIG. 12. The dispersion of the electron-phonon coupling parameter in YPt_2B_2C for (a) the TA_1 branch along the [100] direction, (b) the A_{2u} branch along the Γ-Z direction, and (c) the B_{1g} branch along the Γ-X direction.

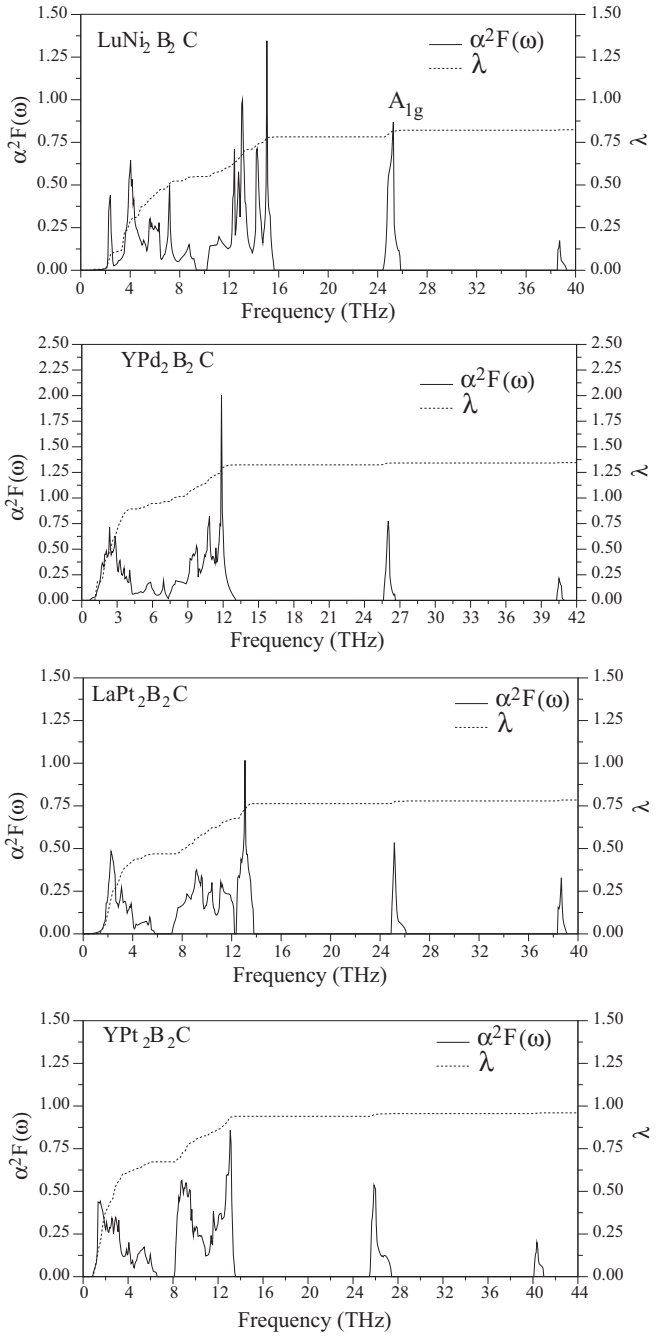

FIG. 13. The calculated electron-phonon spectral function $\alpha^2F(\omega)$ (solid line) and the electron-phonon coupling parameter $\lambda(\omega)$ (dashed line) for RM_2B_2C superconductors.

contribution to $N(E_F)$ while the contributions of R and M to $N(E_F)$ are nearly equal for the other superconductors.

The low-frequency phonon-dispersion curves of $LuNi_2B_2C$ are in good agreement with inelastic-neutron-scattering data. We have confirmed the presence of the experimentally observed softening behavior of the A_{2u} branch in $LuNi_2B_2C$ along the [100] direction close to the zone boundary $G1$. A detailed examination of the Eliashberg function for all studied materials indicates that the acoustic and low-frequency optical-phonon branches make a large contribution within around 70% to average electron-phonon coupling parameter λ. In particular, the anomalous behavior of the A_{2u} phonon mode is essential to the electron-phonon interaction in $LuNi_2B_2C$ rather than the high-frequency A_{1g} branch, which contributes to λ within around 5%. The electron-phonon coupling parameter is found to be 0.78, 0.83, 0.96, and 1.48 for $LaPt_2B_2C$, $LuNi_2B_2C$, YPt_2B_2C, and YPd_2B_2C, respectively. Thus, we can conclude that YPd_2B_2C is a phonon-mediated superconductor with high electron-phonon coupling strength

TABLE IV. The superconducting state parameters for RM_2B_2C and their comparison with available experimental and theoretical results.

Superconductor	$N(E_F)$ (states/eV)	$\omega_{\ln}$ (K)	Θ_D (K)	λ	γ ($\frac{\text{mJ}}{\text{mol K}^2}$)	T_C (K)
$LuNi_2B_2C$						
Present GGA work	3.64	315	380	0.83	15.7	15.94
LDA [52]	4.80					
LDA [57]	3.88					
Experimental [1]						16.5
Experimental [7]			345	0.80	19	16.5
Experimental [18]				0.75	19.5	16.1
Experimental [29]						14.2
Experimental [43]						15.0
YPd_2B_2C						
Present GGA work	2.86	182	218	1.48	16.6	20.60
Experimental [28]						21
$LaPt_2B_2C$						
Present GGA work	2.18	235	283	0.78	9.1	10.40
LDA [56]	2.49					
Experimental [2]					5	10.5
YPt_2B_2C						
Present GGA work	1.96	175	211	0.96	9.0	11.30
Experimental [16]						10

while the remaining materials are phonon-mediated superconductors with medium electron-phonon coupling strength. Using the Allen-Dynes modified McMillian equation with the screened Coulomb pseudopotential parameter $\mu^* = 0.10$, the superconducting critical temperature is found to be 10.40 K for $LaPt_2B_2C$, 11.30 K for YPt_2B_2C, 15.94 K for $LuNi_2B_2C$, and 20.60 K for YPd_2B_2C. These values are in excellent agreement with their experimental values.

ACKNOWLEDGMENTS

This work was supported by the Scientific and Technological Research Council of Turkey (TÜBİTAK) (Project No. MFAG-114F192). Some of the calculations for this project were carried out using the computing facilities on the Intel Nehalem (i7) cluster (ceres) in the School of Physics, University of Exeter, United Kingdom.

[1] R. J. Cava, H. Takagi, H. W. Zandbergen, J. J. Krajewski, W. F. Peck, T. Siegrist, B. Batlogg, R. B. Vandover, R. J. Felder, K. Mizuhashi, J. Lee, H. Eisaki, and S. Uchida, Nature (London) **367**, 252 (1994).

[2] R. J. Cava, B. Batlogg, T. Siegrist, J. J. Krajewski, W. F. Peck, S. Carter, R. J. Felder, H. Takagi, and R. B. van Dover, Phys. Rev. B **49**, 12384 (1994).

[3] R. J. Cava, H. Takagi, H. Eisaki, H. W. Zandbergen, T. Siegrist, B. Batlogg, J. J. Krajewski, W. F. Peck, S. Carter, K. Mizuhaski, J. Lee, S. Uchida, R. Felder, and R. R. Vandover, Physica C **235**, 154 (1994).

[4] T. Siegrist, H. W. Zandbergen, R. J. Cava, J. J. Krajewski, and W. F. Peck, Nature (London) **367**, 254 (1994).

[5] K. Ikushima, J. Kikuchi, H. Yasuoka, R. J. Cava, H. Takagi, J. J. Krajewski, and W. W. Peck, J. Phys. Soc. Jpn. **63**, 2878 (1994).

[6] H. Takagi, R. J. Cava, H. Eisaki, J. Lee, K. Mizuhashi, B. Batlogg, S. Uchida, J. J. Krajewski, and W. F. Peck, Physica C **228**, 389 (1994).

[7] S. A. Carter, B. Batlogg, R. J. Cava, J. J. Krajewski, W. F. Peck, and H. Takagi, Phys. Rev. B **50**, 4216 (1994).

[8] J. S. Kim, W. W. Kim, and G. R. Stewart, Phys. Rev. B **50**, 3485 (1994).

[9] R. Movshovich, M. F. Hundley, J. D. Thompson, P. C. Canfield, B. K. Cho, and A. V. Chubukov, Physica C **227**, 381 (1994).

[10] T. Hasegawa, M. Ogino, G. Takagi, T. Watanabe, M. Nantoh, H. Takagi, S. Uchida, R. J. Cava, and K. Kitawaza, Physica C **235**, 1859 (1994).

[11] C. Murayama, N. Mori, H. Takagi, H. Eisaki, K. Mizuhaski, S. Uchida, and R. J. Cava, Physica C **235**, 2542 (1994).

[12] T. Siegrist, R. J. Cava, J. J. Krajewski, and W. F. Peck, J. Alloys Compd. **216**, 135 (1994).

[13] Y. Y. Sun, I. Rusakova, R. L. Meng, Y. Cao, P. Gautier-Picard, and C. W. Chu, Physica C **230**, 435 (1994).

[14] L. Gao, X. D. Qui, Y. Cao, R. L. Meng, Y. Y. Sun, Y. Y. Xue, and C. W. Chu, Phys. Rev. B **50**, 9445 (1994).

[15] C. Godart, L. C. Gupta, R. Nagarajan, S. K. Dhar, H. Noel, M. Potel, C. Mazumdar, Z. Hossain, C. Levy-Clement, G. Schiffmacher, B. D. Padalia, and R. Vijayaraghavan, Phys. Rev. B **51**, 489 (1995).

[16] F. Yang, N. Tang, J. Wang, W. Qin, Z.-X. Li, and J. Luo, J. Phys. Condens. Matter **7**, 2369 (1995).

[17] G. T. Jeong, J. I. Kye, S. H. Chun, Z. G. Khim, W. C. Lee, and P. C. Canfield, Physica C **253**, 48 (1995).

[18] H. Michor, T. Holubar, C. Dusek, and G. Hilscher, Phys. Rev. B **52**, 16165 (1995).

[19] G. Goll, M. Heinecke, A. G. M. Jansen, W. Joss, L. Nguyen, E. Steep, K. Winzer, and P. Wyder, Phys. Rev. B **53**, R8871 (1996).
[20] F. Bommeli, L. Degiorgi, P. Wachter, B. K. Cho, P. C. Canfield, R. Chau, and M. B. Maple, Phys. Rev. Lett. **78**, 547 (1997).
[21] M. Nohara, M. Isshiki, H. Takagi, and R. J. Cava, J. Phys. Soc. Jpn. **66**, 1888 (1997).
[22] V. N. Narozhnyi, J. Freudenberger, V. N. Kochetkov, K. A. Nenkov, G. Fuchs, A. Handstein, and K.-H. Muller, Phys. Rev. B **59**, 14762 (1999).
[23] J. Zarestky, C. Stassis, A. Goldman, P. Canfield, G. Shirane, and S. Shapiro, Phys. Rev. B **60**, 11932 (1999).
[24] I.-S. Yang, M. V. Klein, S. L. Cooper, P. C. Canfield, B. K. Cho, and S.-I. Lee, Phys. Rev. B **62**, 1291 (2000).
[25] G. Ghosh, A. D. Ahincure, R. Nagarajan, C. Godart, and L. C. Gupta, Phys. Rev. B **63**, 212505 (2001).
[26] S. Manalo, H. Michor, M. El-Hagary, G. Hilscher, and E. Schachinger, Phys. Rev. B **63**, 104508 (2001).
[27] S. J. Lee, B. K. Cho, P. C. Canfield, and D. W. Lynch, Phys. Rev. B **63**, 233103 (2001).
[28] H. Bitterlich, W. Löser, H.-G. Lindenkreuz, and L. Schultz, J. Alloys Compd. **325**, 285 (2001).
[29] A. Andreone, A. Cassinese, L. Gianni, M. Iavarone, F. Palomba, and R. Vaglio, Phys. Rev. B **64**, 100505(R) (2001).
[30] K. Izawa, K. Kamata, Y. Nakajima, Y. Matsuda, T. Watanabe, M. Nohara, H. Takagi, P. Thalmeier, and K. Maki, Phys. Rev. Lett. **89**, 137006 (2002).
[31] J. L. Zarestky, C. Stassis, A. I. Goldman, P. C. Canfield, G. Shirane, and S. M. Shapiro, J. Phys. Chem. Solids **63**, 811 (2002).
[32] D. Bintley and P. J. Meeson, Physica C **388-389**, 181 (2003).
[33] K. Kamata, K. Izawa, Y. Nakajima, Y. Matsuda, T. Watanabe, M. Nohara, H. Takagi, H. Takeya, K. Hirata, P. Thalmeier, and K. Maki, J. Low Temp. Phys. **131**, 1095 (2003).
[34] G. Fuchs, K.-H. Müller, S.-L. Drechsler, S. Shulga, K. Nenkov, J. Freudenberger, G. Behr, D. Souptel, A. Handstein, A. Wälte, D. Lipp, and L. C. Gupta, Physica C **408**, 107 (2004).
[35] P. Raychaudhuri, D. Jaiswal-Nagar, G. Sheet, S. Ramakrishnan, and H. Takeya, Phys. Rev. Lett. **93**, 156802 (2004).
[36] M. Udagawa, Y. Yanase, and M. Ogata, Phys. Rev. B **71**, 024511 (2005).
[37] L.-S. Hsu, C.-J. Chen, and M.-D. Lan, J. Alloys Compd. **397**, 23 (2005).
[38] C. L. Huang, J.-Y. Lin, C. P. Sun, T. K. Lee, J. D. Kim, E. M. Choi, S. I. Lee, and H. D. Yang, Phys. Rev. B **73**, 012502 (2006).
[39] B. Bergk, O. Ignatchik, A. D. Bianchi, M. Jäckel, J. Wosnitza, J. Perenboom, and P. C. Canfield, Physica C **460-462**, 630 (2007).
[40] B. Bergk, V. Petzold, H. Rosner, S.-L. Drechsler, M. Bartkowiak, O. Ignatchik, A. D. Bianchi, I. Sheikin, P. C. Canfield, and J. Wosnitza, Phys. Rev. Lett. **100**, 257004 (2008).
[41] S. B. Dugdale, C. Utfeld, I. Wilkinson, J. Laverock, Z. Major, M. A. Alam, and P. C. Canfield, Supercond. Sci. Technol. **22**, 014002 (2009).
[42] T. Baba, T. Yokoya, S. Tsuda, T. Watanabe, M. Nohara, H. Takagi, T. Oguchi, and S. Shin, Phys. Rev. B **81**, 180509 (2010).
[43] X. Lu, W. K. Park, S. Yeo, K.-H. Oh, S.-I. Lee, S. L. Budko, P. C. Canfield, and L. H. Greene, Phys. Rev. B **83**, 104519 (2011).
[44] D. Varshney and R. K. Jain, Mod. Phys. Lett. B **26**, 1150045 (2012).
[45] A. E. Karkin, Yu. N. Akshentsev, and B. N. Goshchitskii, JETP Lett. **97**, 347 (2013).
[46] D. D. Lawrie and J. P. Franck, Physica C **245**, 159 (1995).
[47] K. O. Cheon, I. R. Fisher, and P. C. Canfield, Physica C **312**, 35 (1999).
[48] V. G. Hadjiev, L. N. Bozukov, and M. G. Baychev, Phys. Rev. B **50**, 16726 (1994).
[49] P. Dervenagas, M. Bullock, J. Zarestky, P. Canfield, B. K. Cho, B. Harmon, A. I. Goldman, and C. Stassis, Phys. Rev. B **52**, R9839(R) (1995).
[50] H.-J. Park, H.-S. Shin, H.-G. Lee, I.-S. Yang, W. C. Lee, B. K. Cho, P. C. Canfield, and D. C. Johnston, Phys. Rev. B **53**, 2237 (1996).
[51] F. Weber, S. Rosenkranz, L. Pintschovius, J. P. Castellan, R. Osborn, W. Reichardt, R. Heid, K. P. Bohnen, E. A. Goremychkin, A. Kreyssig, K. Hradil, and D. L. Abernathy, Phys. Rev. Lett. **109**, 057001 (2012).
[52] L. F. Mattheiss, Phys. Rev. B **49**, 13279 (1994).
[53] L. F. Mattheiss, T. Siegrist, and R. J. Cava, Solid State Commun. **91**, 587 (1994).
[54] W. E. Pickett and D. J. Singh, Phys. Rev. Lett. **72**, 3702 (1994).
[55] R. Coehoorn, Physica C **228**, 331 (1994).
[56] D. J. Singh, Phys. Rev. B **50**, 6486 (1994).
[57] H. Kim, C.-D. Hwang, and J. Ihm, Phys. Rev. B **52**, 4592 (1995).
[58] R. Weht, O. M. Cappannini, C. O. Rodriguez, and N. E. Christensen, Physica C **260**, 125 (1996).
[59] O. M. Cappannini, C. O. Rodriguez, and N. E. Christensen, Physica C **306**, 101 (1998).
[60] P. Ravindran, A. Kjekshus, H. Fjellvag, P. Puschnig, C. Ambrosch-Draxl, L. Nordström, and B. Johansson, Phys. Rev. B **67**, 104507 (2003).
[61] W. Reichardt, R. Heid, and K. P. Bohnen, J. Supercond. **18**, 759 (2005).
[62] H. Y. Uzunok, H. M. Tütüncü, S. Özer, Ş. Uğur, and G. P. Srivastava, Solid State Commun. **206**, 1 (2015).
[63] P. Giannozzi, S. Baroni, N. Bonini, M. Calandra, R. Car, C. Cavazzoni, D. Ceresoli, G. L. Chiarotti, M. Cococcioni, I. Dabo, A. D. Corso, S. de Gironcoli, S. Fabris, G. Fratesi, R. Gebauer, U. Gerstmann, C. Gougoussis, A. Kokalj, M. Lazzeri, L. Martin-Samos, N. Marzari, F. Mauri, R. Mazzarello, S. Paolini, A. Pasquarello, L. Paulatto, C. Sbraccia, S. Scandolo, G. Sclauzero, A. P. Seitsonen, A. Smogunov, P. Umari, and R. M. Wentzcovitch, J. Phys. Condens. Matter **21**, 395502 (2009).
[64] J. P. Perdew, K. Burke, and M. Ernzerhof, Phys. Rev. Lett. **77**, 3865 (1996).
[65] R. Stumpf, X. Gonge, and M. Scheffler, *A List of Separable, Norm-conserving, Ab Initio Pseudopotentials* (Fritz-Haber-Institut, Berlin, 1990).
[66] D. Vanderbilt, Phys. Rev. B **41**, 7892 (1990).
[67] A. M. Rappe, K. M. Rabe, E. Kaxiras, and J. D. Joannopoulos, Phys. Rev. B **41**, 1227 (1990).
[68] W. Kohn and L. J. Sham, Phys. Rev. **140**, A1133 (1965).
[69] H. J. Monkhorst and J. D. Pack, Phys. Rev. B **13**, 5188 (1976).
[70] A. B. Migdal, Zh. Eksp. Teor. Fiz. **34**, 996 (1958).
[71] G. M. Eliashberg, Sov. Phys. JETP **11**, 696 (1960).
[72] P. B. Allen, Phys. Rev. B **6**, 2577 (1972).
[73] P. B. Allen and R. C. Dynes, Phys. Rev. B **12**, 905 (1975).
[74] V. Z. Kresin and G. O. Zaitsev, Sov. Phys. JETP **47**, 983 (1978).
[75] S. Y. Savrasov, D. Y. Savrasov, and O. K. Andersen, Phys. Rev. Lett. **72**, 372 (1994).

[76] S. Y. Savrasov and D. Y. Savrasov, Phys. Rev. B **54**, 16487 (1996).
[77] A. Y. Liu and A. A. Quong, Phys. Rev. B **53**, R7575 (1996).
[78] R. Bauer, A. Schmid, P. Pavone, and D. Strauch, Phys. Rev. B **57**, 11276 (1998).
[79] S. Baroni, S. de Gironcoli, and A. Dal Corso, Rev. Mod. Phys. **73**, 515 (2001).
[80] F. D. Murnaghan, Proc. Natl. Acad. Sci. (USA) **30**, 244 (1944).
[81] E. I. Isaev, R. Ahuja, S. I. Simak, A. I. Lichtenstein, Y. K. Vekilov, B. Johansson, and A. I. Abrikosov, Phys. Rev. B **72**, 064515 (2005).
[82] E. I. Isaev, S. I. Simak, I. A. Abrikosov, R. Ahuja, Y. K. Katsnelson, A. I. Lichtenstein, and B. Johansson, J. Appl. Phys. **101**, 123519 (2007).
[83] H. M. Tütüncü, S. Bağcı, G. P. Srivastava, and A. Akbulut, J. Phys. Condens. Matter **24**, 455704 (2012).